Electronic Supplementary Material (ESI) for Lab on a Chip
This journal is © The Royal Society of Chemistry 2012

Supporting Information for

"Quantitative full-colour transmitted light microscopy and dyes for concentration mapping and measurement of diffusion coefficients in microfluidic architectures"

Martinus H. V. Werts,*[a,b] Vincent Raimbault,[c] Rozenn Texier-Picard,[a,d] Rémi Poizat, [a,b] Olivier Français,[b,e] Laurent Griscom,[a,b] and Julien R. G. Navarro[a,b]

[a] *Ecole Normale Supérieure de Cachan-Bretagne, UEB, Campus de Ker Lann, F-35170 Bruz, France*

[b] *CNRS, SATIE (UMR8029), ENS Cachan-Bretagne, UEB, Campus de Ker Lann, F-35170 Bruz, France*

[c] *CNRS, IMS (UMR5218), Université de Bordeaux, 351 cours de la Libération, F-33405 Talence Cedex, France*

[d] *CNRS, IRMAR (UMR6625), ENS Cachan-Bretagne, UEB, Campus de Ker Lann, F-35170 Bruz, France*

[e] *Ecole Normale Supérieure de Cachan, 61 Avenue du Président Wilson, F-94235 Cachan Cedex, France*

* corresponding author, e-mail: martinus.werts@bretagne.ens-cachan.fr

This journal is © The Royal Society of Chemistry 2012

SI-1. Dose-repsonse (concentration-optical density) dilution plots for several dyes

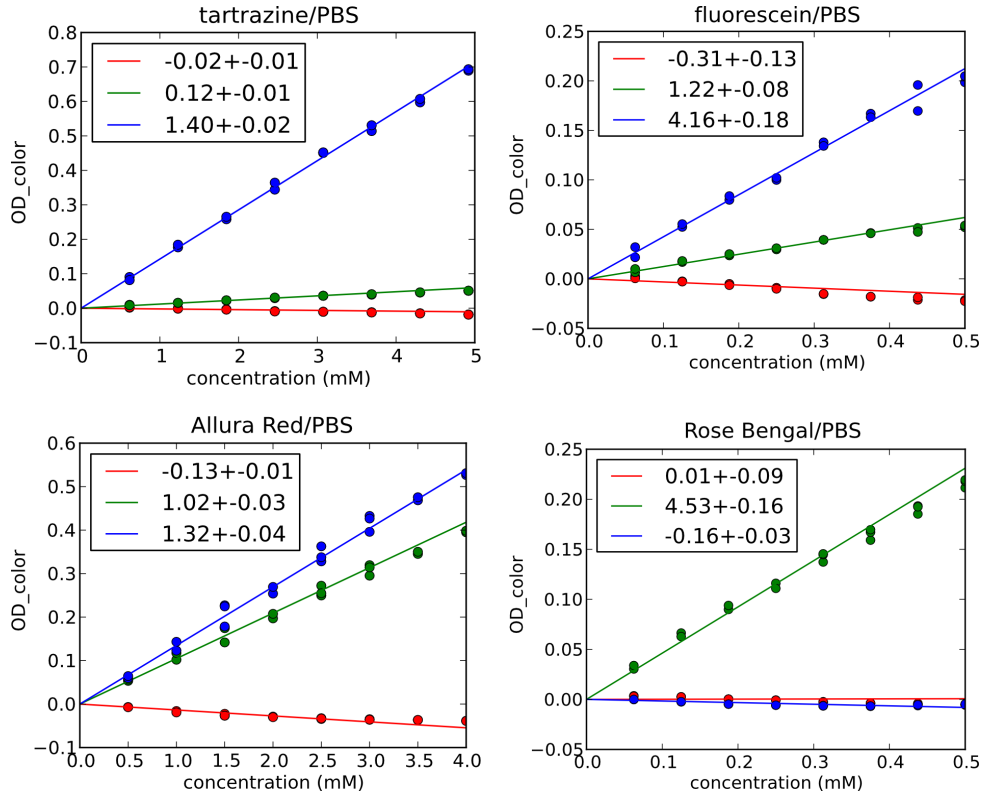

Figure SI-1. *Typical calibration plots for quantitative transmitted light microscopy. The insets show the effective molar absorption coefficients (EMACs) for each colour. Per colour-channel optical densities obtained by analysing digital optical micrographs of channels filled with varying concentrations of dye in PBS solution. Microfluidic channel heights were in the range 102...110 µm (measured by a stylus profilometer).*

This journal is © The Royal Society of Chemistry 2012

SI-2. Effective molar absorption coefficients (EMACs) obtained on an alternative microscope set-up

The table below contains EMACs for three dyes in PBS determined on an alternative microscope setup, that includes a low-cost colour CMOS camera, instead of the colour CCD on the main system. The dilution curves are linear also on this system, and concentration mapping is possible.

	$EMAC_{RED}$ / $mM^{-1}mm^{-1}$	$EMAC_{GREEN}$ / $mM^{-1}mm^{-1}$	$EMAC_{BLUE}$ / $mM^{-1}mm^{-1}$
Tartrazine	0.00 ± 0.01	0.04 ± 0.01	0.6 ± 0.1
Allura Red	0.14 ± 0.02	0.6 ± 0.1	1.1 ± 0.1
Fast Green	4.9 ± 0.2	1.9 ± 0.1	1.3 ± 0.1

While of the same order of magnitude, and following similar trends, the EMACs are up to 70% lower. We noticed that colour separation in the lower cost CMOS system is less efficient, leading to less performance in particular in the blue channel. Yellow dye Tartrazine showed linear behaviour only up to 2 mM (100 μm path length). Fast Green and Allura Red did not show deviations from linearity. These results indicate the necessity of a 'per microscrope' calibration. They also indicate that for lower performance systems, the red and green channels (cyan and magenta dyes) are to be preferred.

SI-3. Truncation behaviour of Fourier-based diffusion formula

Here we study the effect of truncating the series in Equation 12. For a single term we obtain

$$\frac{OD_A - OD_B}{OD_A + OD_B} \approx \frac{8}{\pi^2} \exp\left(\frac{-D\pi^2}{w^2} t\right)$$

This approximated form can be cast into a linearised form (Equation 16), that allows for facile determination of the diffusion coefficient from a linear plot (e.g. bottom graph of Figure 5). Adding more terms we obtain

$$\frac{OD_A - OD_B}{OD_A + OD_B} \approx \frac{8}{\pi^2} \left(\exp\left(\frac{-D\pi^2}{w^2} t\right) + \frac{1}{9} \exp\left(\frac{-9D\pi^2}{w^2} t\right)\right)$$

and so on.

Figure SI-2 shows the effect of the number of terms used in the numerical evaluation of Equations 11 and 12. At higher flow speeds (low values of τ) more terms are needed for an

accurate description, but as long as $C_B / C_A > 0.2$ ($\ln \xi < -0.4$) a single term is sufficient , giving a range of validity for the linearized form in Equation 4-9. Truncation errors only show up when $\ln \xi > -0.4$.

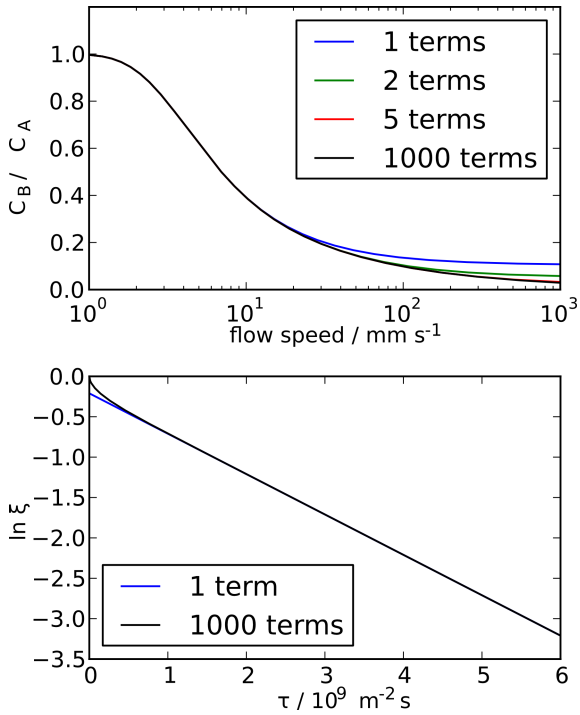

Figure SI-2. *Truncation behaviour of the numerical evaluation of Equations 11 and 12 for $D = 5 \times 10^{-10}$ m^2 s^{-1}, with channel height, width, length 100 µm, 200 µm, 50 mm, respectively. In the bottom part, two evaluations of Equation 11 are plotted in the style of linearised Equation 16, in order to see where this linearity is lost due to the necessity to include more Fourier terms.*

SI-4. Comparison of 'Fourier'-type solution (this work, Equations 9, 11, 12, 13) with 'erf'-type solution (Equation 8)

It is interesting to compare the results of the Fourier-based solution of the diffusion equation used in this work (Equations 9, 11, 12, 13) with the 'error function' based solution often employed in the analysis of diffusion in T-sensor or H-filter architectures (Equation 8). For such a comparison, we evaluate ξ as defined in Equation 5, using concentration profiles from this 'error function' formalism (Equation 8). We then obtain the following "erf"-based formula (Equation SI-1).

$$\xi_{\mathrm{erf}} = \frac{C_A - C_B}{C_A + C_B} = \frac{2}{w} \int_0^{w/2} \mathrm{erf}\left(\frac{ay}{\sqrt{t}}\right) dy \quad \text{with} \quad a = \frac{\pi}{w\sqrt{D}} \qquad \text{(SI-1)}$$

This journal is © The Royal Society of Chemistry 2012

Figure SI-3 shows that for small τ (high flow-rates, short diffusion times) the "Fourier" solution and the "erf" solution converge. However, at larger τ, significant deviations between the two solutions occur, with the "Fourier" solution used in this work describing more reliably the experimental data. The deviation of the "erf" solution at longer diffusion times is caused by the initial assumption of the interaction between two inifinitely wide flows, whereas the actual channel width is finite. This finite width is reliably taken into account by the "Fourier" solution. Moreover, for longer interaction times, one term of the Fourier series is sufficient for an accurate description, making it possible to cast the behaviour of the Péclet-O-Matic in the simplified, linear form of Equation 16.

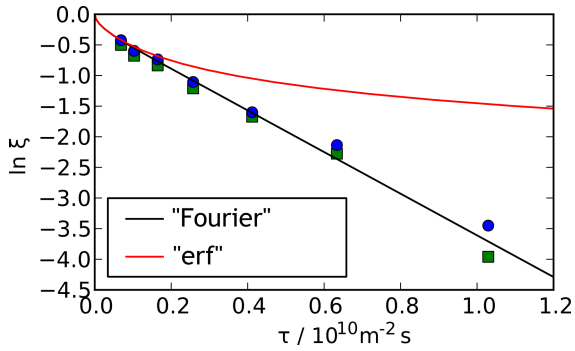

Figure SI-3. *Theoretical curves obtained using Equation 12 (solid line, black) and Equation SI-1 (red). In both cases the diffusion coefficient D was set to 3.4 x 10^{-10} m^2 s^{-1}. The blue and green squares are experimental data for Allura Red in PBS (same date as Figure 5, main text)*

This journal is © The Royal Society of Chemistry 2012

SI-5. Concentration profiles of gold nanoparticles (AuTA) diffusing between laminar flows

Figure SI-4 shows the diffusion of 13 nm diameter gold nanoparticles between two laminar flows. The intense optical absorption by these particles allows for their observation in optical microscopy. Figure SI-5 shows typical concentration profiles extracted from these images, and how well they are described by the Fourier solution Equation 9.

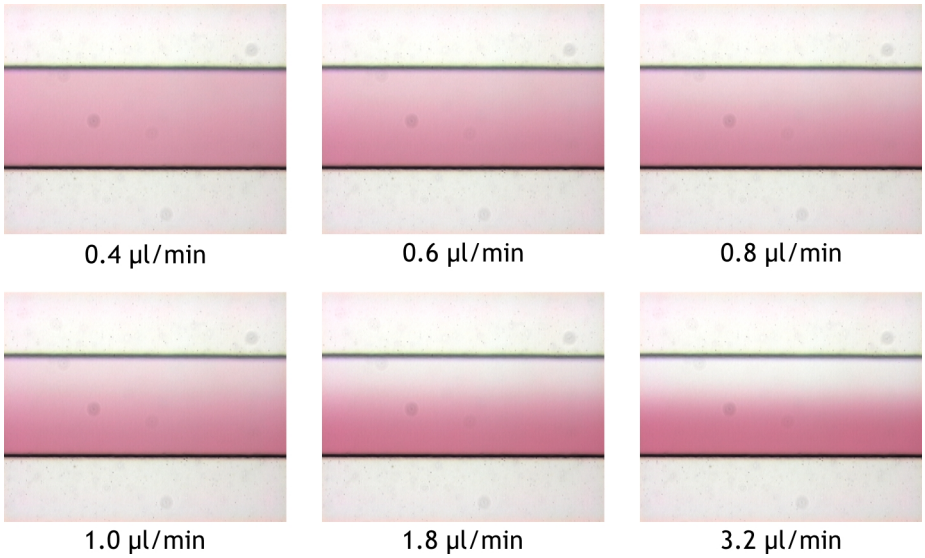

Figure SI-4. *Transmitted-light colour micrographs (10x, NA 0.22 objective) of the channel with two interacting laminar flows after 54 mm (width = 200 µm, height = 105 µm). This corresponds to a region just before "2" in Figure 2 (main text). One flow initially contained all of the AuTA nanoparticles in 1mM NaOH, the other only solvent (1mM NaOH). The flow rate was varied, leading to different interaction times in the channel. The coloration is due to the strong gold nanoparticle plasmon resonance, enabling detection at low concentrations. At high flow rates, the diffusion of the gold nanoparticles is incomplete after 54 mm.*

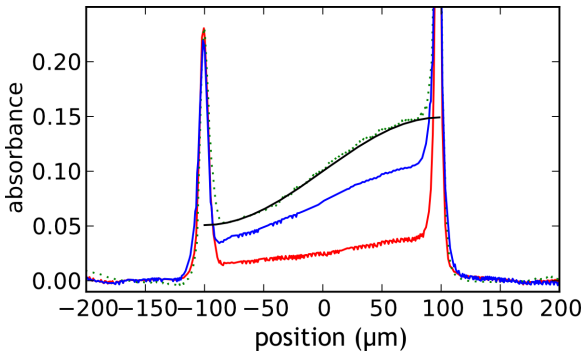

Figure SI-5. *Red, green and blue absorbance profiles for diffusing gold nanoparticles extracted from the microscopic image recorded at 0.6 µl min^{-1} (Figure SI-4). The black line is a theoretical concentration profile calculated using Equation 9, and a diffusion coefficient 3.5 x 10^{-11} m^2 s^{-1}, indicating to validity of Equation 9 under the experimental conditions. The concentration profiles at other flow rates also were well described using Equation 9 and D = 3.5 x 10^{-11} m^2 s^{-1}.*

This journal is © The Royal Society of Chemistry 2012

SI-6. Colour image analysis of a passive mixer device mixing two dyes

The panoramic view of the staggered herringbone mixer (SHM, Figure SI-6) has been constructed from the raw digital colour images, without dark subtraction, nor flatfield-correction unlike the other panoramic images in this work (Figure 7, main text, and Figure SI-7).

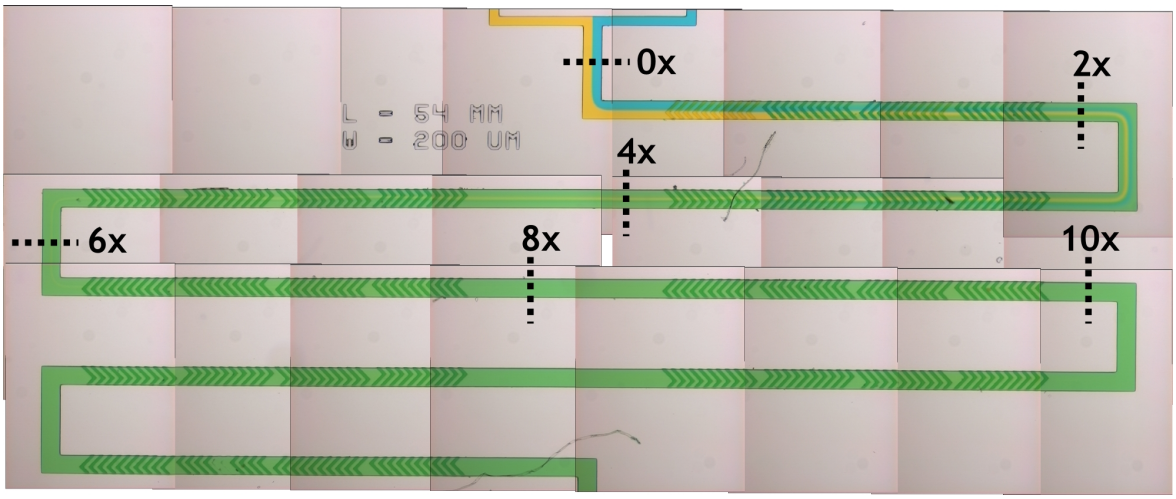

***Figure SI-6**. Panoramic multi-image view (2.5x, NA 0.07 objective) of device incorporating a 16-cycle staggered herringbone mixer, mixing 0.9 mM fast green and 4.6 mM tartrazine in PBS, at a total flow rate of 14 µl min^{-1}. The dashed lines labeled "0x" etc. indicate the places where the dye concentration profiles have been extracted for the graphs in Figure 6 (main text).*

This journal is © The Royal Society of Chemistry 2012

SI-7. Panoramic image of device without staggered herringbone motif

Figure SI-7 has been included as a complement to Figure SI-6, in order to illustrate the effect of the SHM motif on fluid mixing. The panoramic image of Figure SI-7 demonstrates the effect of flat-field correction when compared to Figure SI-6. Three colour optical densities can be readily extracted by applying Equation 4, with a constant value for $\mathbf{I}_0$.

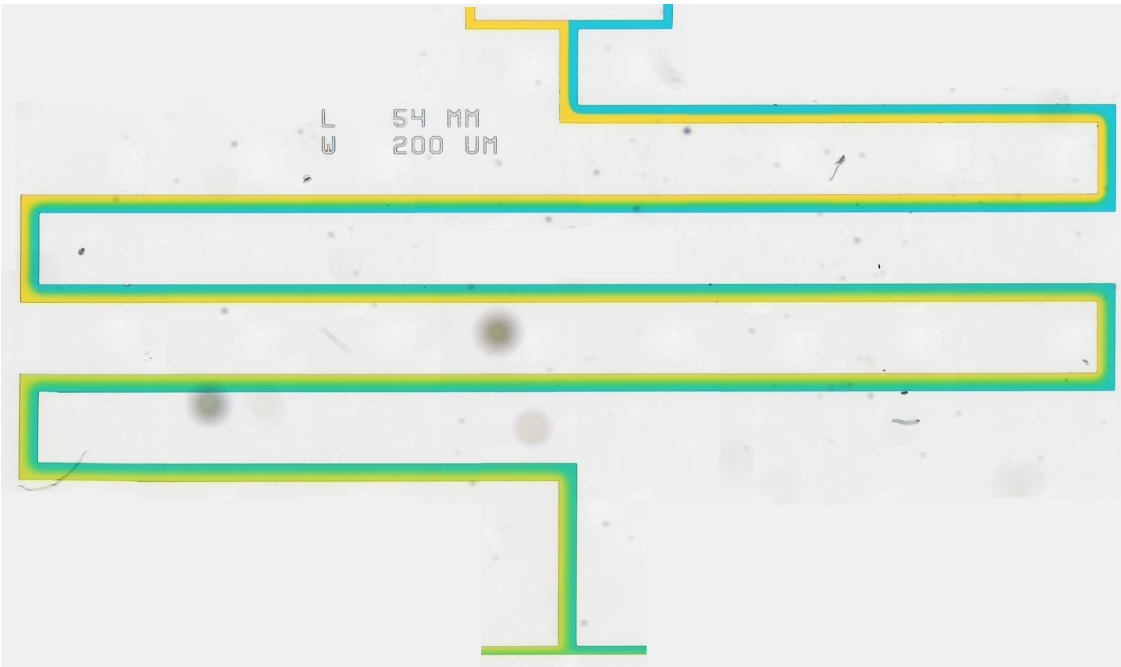

Figure SI-7*. Panoramic multi-image view (2.5x, NA 0.07 objective) of the Péclet-O-Matic without any staggered herringbone mixer, at a flow rate of 14 µl min^{-1}. Before compiling the panorama, all images were corrected for background and flatfield.*